Therapeutic Advances in Neurological Disorders Review

Imaging in neuro-oncology

Hari Nandu, Patrick Y. Wen and Raymond Y. Huang

Ther Adv Neurol Disord
2018, Vol. 11: 1–19
DOI: 10.1177/1756286418759865

***Abstract*:** Imaging plays several key roles in managing brain tumors, including diagnosis, prognosis, and treatment response assessment. Ongoing challenges remain as new therapies emerge and there are urgent needs to find accurate and clinically feasible methods to noninvasively evaluate brain tumors before and after treatment. This review aims to provide an overview of several advanced imaging modalities including magnetic resonance imaging and positron emission tomography (PET), including advances in new PET agents, and summarize several key areas of their applications, including improving the accuracy of diagnosis and addressing the challenging clinical problems such as evaluation of pseudoprogression and anti-angiogenic therapy, and rising challenges of imaging with immunotherapy.

Keywords: brain tumor, glioblastoma, 18F-FLT, 18F-FET, 18F-DOPA, PET-CT, radiomics, iRANO, immunotherapy, neuro-oncology

Received: 20 October 2017; revised manuscript accepted: 18 January 2018.

Correspondence to:
Raymond Huang
Department of Radiology, Brigham and Women's Hospital, 75 Francis Street, Boston, MA 02445, USA
ryhuang@bwh.harvard.edu

Hari Nandu
Department of Radiology, Brigham and Women's Hospital, Boston, MA, USA

Patrick Y. Wen
Dana-Farber Cancer Institute, Boston, MA, USA

Introduction

The roles of imaging in neuro-oncology primarily consist of diagnosis, prognosis, and treatment response assessment of central nervous system (CNS) tumors. Imaging assessment is currently an important surrogate endpoint for clinical trials. With ongoing evaluation and discovery of novel treatment agents, including immunotherapy agents, the ability to accurately assess progression and discern treatment-related changes is a central goal of neuro-oncologic imaging. In this review, we will summarize several clinically available imaging techniques as well as some novel methods under development, and provide an up-to-date review of some clinical challenges in treatment of glioblastomas where imaging can have important roles.

Update of advanced imaging techniques in neuro-oncology

Diffusion-weighted magnetic resonance imaging (DW-MRI) can characterize tissues based on the differences in the degree of free movement of protons. It has been shown that the cellularity or cell density of tumor is associated with apparent diffusion coefficient (ADC), a calculated metric from DW-MRI.[1] This property allows one to distinguish between both tumor subtypes and tumor grades (low *versus* high). More recently, high *b*-value DW-MRI, using a *b*-value >3000 s/mm^2, has been demonstrated to be superior to standard DW-MRI in distinguishing tumor tissue from normal brain parenchyma.[2] DW-MRI data can also be further quantified to generate imaging markers using techniques such as diffusion kurtosis imaging (DKI),[3] histogram curve-fitting,[4] and functional diffusion map (fDM).[5] Restriction spectrum imaging (RSI) is an DW-MRI technique that can isolate the diffusion properties of tumor cells from extracellular process such as edema, potentially improving specificity of tumor detection and characterization.[6] Diffusion tensor imaging (DTI) measures the directionality of proton motion as fractional anisotropy (FA), which is often altered in the presence of brain tumors.[7] Applications of these methods will be reviewed in the following sections.

Perfusion-weighted magnetic resonance imaging (PW-MRI) techniques assess blood flow to tissue by calculating parameters derived from the time–intensity curve. Using the normal brain as reference, these techniques can detect pathological alterations of tissue vascularity that commonly occur among brain tumors due to increased vascular permeability as well as intravascular blood volume because of tumor-induced angiogenesis. Dynamic susceptibility contrast magnetic resonance imaging (DSC-MRI) quantifies first-pass bolus of paramagnetic contrast agent,[8,9] and is currently the most common perfusion-weighted

imaging method in clinical use. Dynamic contrast enhanced magnetic resonance imaging (DCE-MRI) can characterize vascular permeability within or surrounding tumors by using pharmacokinetic models to quantify the movement of contrast agents crossing the blood–brain barrier.[10–12] DCE-MRI has an advantage over DSC-MRI due to its greater signal-to-noise ratio and spatial resolution, although imaging acquisition time is also longer. Perfusion imaging measurements are highly dependent on imaging acquisition parameters and postprocessing techniques, including variations in postprocessing software tools.[13] Clinical application of this technique therefore requires efforts in standardization, particularly in multicenter settings.

Magnetic resonance spectroscopy (MRS) measures concentrations of metabolites within tissues noninvasively.[14] The single-voxel spectroscopy (SVS) method collects average MRS data within a target region of interest selected on standard MRI images. The multivoxel spectroscopy (MVS) method can obtain two- or three-dimensional maps of the region of interest to detect voxel-wise spatial changes of specific metabolites. Both SVS and MVS approaches have been evaluated in tumor diagnosis, grading, pre-therapy planning and post-therapy assessment. One major limitation of the technique is its operator dependency, requiring experienced staff to manually select regions of interest during acquisition. It is also less sensitive to lesions with volume <1.5 cm^3.

18F-fluorodeoxyglucose (18F-FDG) positron emission tomography (PET) is an important imaging tool in oncology.[15] Similar to systemic cancers, brain tumors often exhibit increased metabolic activity resulting in elevated 18F-FDG uptake that can be detected by PET.[16] The role of FDG-PET in brain tumor imaging, however, has been quite limited due to its relative lack of specificity and high background uptake by the normal brain. This limitation is particularly important for small lesions, as currently the resolution of PET imaging is limited to 5 mm. More recently, amino acid PET tracers including ^{11}C-methionine, 18F-fluorothymidine (FLT), 18F-fluoro-ethyl-tyrosine (FET), and 18F-dihydroxyphenylalanine (DOPA) have been developed and evaluated for brain tumor imaging. This class of radiotracers is avidly taken up by malignant brain tumors that have higher cellular proliferation compared to the normal brain.[17–20] The advantage of high lesion-to-background uptake ratio makes amino acid PET suitable for imaging of brain tumors, including applications such as predicting tumor grade, detecting recurrent tumor, and assessing treatment response. Novel PET radiotracer (18) F-fluoromisonidazole (18F-FMISO) has been evaluated as a marker of tissue hypoxia before and after treatment.[21,22]

With increasing computing speed and availability of pre-engineered algorithms, imaging data can be analyzed for voxel-level intensity variations to generate texture-type features that can be correlated with tumor biology or treatment response. This approach can be applied to any imaging modality individually or simultaneously through spatial co-registration. As a result, imaging features can be regarded as tumor phenotypes and this type of biomarker can be summarized by the term 'radiomics'.[23] Screening or combining a large number of radiomic features allows generation of models that can aid oncologic diagnosis, prognostication, and treatment response prediction. This approach has been successful in a number of systemic cancers.[24–28] The radiomic approach is particularly suitable for evaluating high-grade gliomas, a tumor type that is well known for its genetic heterogeneity and highly complex imaging phenotypes.

Preoperative evaluation of brain tumor: diagnosis and prognosis

Imaging plays a key role in the diagnosis of brain tumors and has become one routine management step during preoperative evaluation to aid determination of tumor grade and prognosis. It can also provide important spatial information on tumor tissue characteristics for some tumor subtypes that can influence surgical and radiation treatment planning. In addition, imaging has shown increasing ability to detect tumor genetic profile that can further provide valuable prognostic and predictive information for optimal treatment planning. Finally, imaging findings are often combined with clinical data such as age, gender, and presenting symptoms and signs to increase the accuracy of diagnosis for various tumor types, as well as identifying non-tumor mimics.

One common clinical dilemma during preoperative diagnosis of brain tumors is to distinguish between high-grade glioma and lymphoma. Standard management of CNS lymphoma is non-surgical and biopsy is the preferred approach if lymphoma is suspected preoperatively, whereas

maximal surgical resection provides the best prognosis for high-grade glioma. On conventional imaging sequences, these tumor types commonly exhibit contrast enhancement and peritumoral edema, which make it challenging to differentiate. Lymphomas typically exhibit low ADC values due to high cellularity.[29,30] However, this histological feature can be seen in high-grade gliomas and metastases.

Quantitatively, the FA and ADC values of primary cerebral lymphoma are significantly lower than those of glioblastoma.[31,32] There is also evidence that DSC-MRI and DCE-MRI parameters of the enhancing regions of the tumor can discriminate between lymphomas and glioblastomas as well as between lymphomas and metastasis,[32,33] although a direct comparison of DCE-MRI and DW-MRI shows that ADC measurement is superior to DCE-MRI in differentiating the two tumor types.[34] Detection of intratumoral microhemorrhage using the susceptibility-sensitive MRI technique also allows differentiation of glioblastoma and primary CNS lymphomas.[35] Texture features generated from post-contrast images of lymphoma and glioblastoma also allow diagnostic differentiation.[36]

Analysis of nonenhancing signal abnormalities surrounding brain lesions can provide independent diagnostic information. ADC values measured within fluid-attenuated inversion recovery (FLAIR) abnormalities surrounding the enhancing regions can differentiate high-grade gliomas from solitary metastases.[37,38] The difference could be due to the presence of tumor infiltration by glioma, resulting in higher cellularity than tumor-induced edema.[39] This is also supported by MRS and DSC-MRI measurements of the peritumoral region showing higher choline to N-acetylaspartic acid (NAA) ratio and greater vascularity among high-grade gliomas compared to brain metastases.[32,40,41] Combined evaluation of both the enhancing and nonenhancing regions can potentially enhance diagnostic accuracy.[32,42] Beyond the margins of signal abnormalities outlined by conventional MRI, including T1- and T2-weighted imaging, MRS can identify regions of brain containing tumor and improve surgical resection and patient outcome.[43,44]

Molecular data of gliomas have demonstrated prognostic significance and have been incorporated into the 2016 World Health Organization (WHO) criteria.[45] The imaging characteristics of brain tumors can be directly related to a specific set of tumor genomics, providing opportunities to noninvasively predict tumor genotype preoperatively. Radiomic models have been developed based on conventional MRI, DTI, and DSC-MRI for predicting gene expression profiles of newly diagnosed glioblastomas.[46] Specific genetic alterations of tumors can also be predicted by analysis of MRI data and predictive models have been generated for O6-methylguanine-DNA methyltransferase (MGMT) methylation status,[47,48] epidermal growth factor (EGFR) amplification status,[25,49] and EGFR receptor variant III status.[50] Isocitrate dehydrogenase 1/2 (IDH) mutations are commonly present in low-grade gliomas as well as secondary glioblastomas. These mutant tumors accumulate 2-hydroxyglutarate (2HG), an onco-metabolite that can be detected by MRS (Figure 1).[51] Measurement of 2HG concentration allows diagnosis of IDH mutant tumor preoperatively and also opportunities to monitor tumor activity during treatment.[52,53] Static and dynamic FET-PET measurements have also been correlated with IDH and 1p/19q status.[54] More recently, multimodal MRI imaging can be evaluated by machine learning algorithms to generate predictive models for IDH status in gliomas.[55–57]

Prognosis and tumor-grading

A prognostic imaging marker can be identified by correlating the marker with histological grading of the tumor or with patients' clinical outcomes. With its noninvasive nature, imaging prognosticators can benefit patient care throughout the clinical course of disease, most importantly at the time of diagnosis for surgical or radiation planning, as well as early after treatment to determine efficacy. In patients with glioblastomas, the most common malignant primary brain tumors, the median survival is 14–16 months with best available standard treatment.[58] The ability to predict progression-free or overall-survival outcomes for these patients can impact their treatment decision-making.

Compared to low-grade gliomas, high-grade gliomas demonstrate higher cellularity on DW-MRI,[59,60] higher choline to NAA ratio on MRS,[60–64] high relative blood volume on DSC-MRI,[60,65,66] and increased uptakes on FDG and FLT PET.[67–69] Increased time activity curves of FET in tumor cells also have been shown to correlate with high-grade tumor.[70,71] Radiomic models predicting WHO grade of gliomas have been generated using conventional MRI sequences.[72]

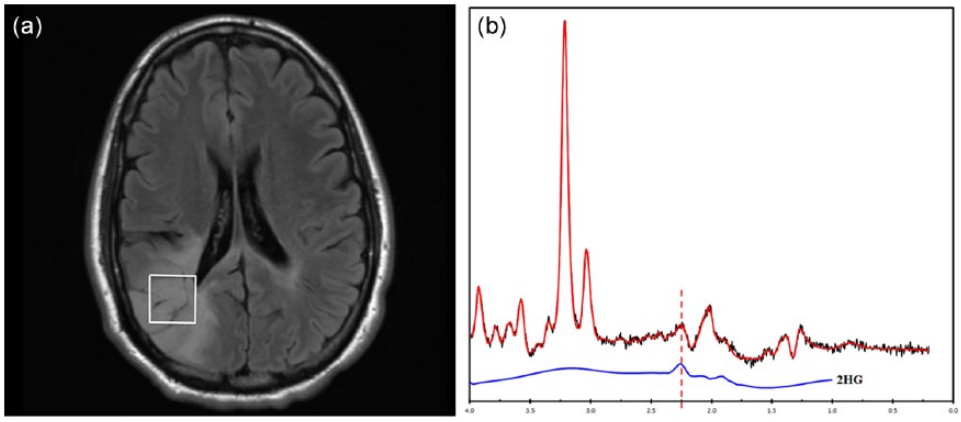

Figure 1. 2-hydroxyglutarate (2HG) magnetic resonance spectroscopy. (a) Axial FLAIR image of a 34-year-old woman with a right parietal lobe nonenhancing mass. (b) Single-voxel magnetic resonance performed at 3T, TE of 97 ms, demonstrates a peak at 2.3 ppm (dashed line), indicating presence of 2HG.
Image provided courtesy of Drs. Alexander Lin and Min Zhou.

For glioblastomas, a number of imaging modalities can provide prognostic information of overall survival, including DSC-MRI,[73–75] DCE-MRI,[76] high b-value DW-MRI,[77] and FET-PET. Early time to peak on time activity curves of FET-PET has been shown to correlate with worse outcome in patients with high-grade glioma.[70] Furthermore, longer median time to peak was found to correlate with better outcomes with FET-PET in IDH1/2 mutant and1p/19q non co-deleted subgroup of patients with glioma.[71] Multiparametric volumetric analysis combining data from diffusion and perfusion imaging of patients with glioblastomas can predict survival.[78] A prospective evaluation of several imaging modalities including DCE-MRI, DSC-MRI, and 18F-FMISO PET prior to standard chemoradiation treatment in newly diagnosed glioblastoma revealed poor prognosis associated with increased tumor perfusion, vascular volume, vascular permeability, and hypoxia.[22] Prognostic models based on radiomic features have been generated from preoperative imaging of newly diagnosed glioblastomas.[46,79–86]

Imaging can provide location-specific diagnostic or prognostic information within brain tumors to identify regions associated with higher tumor grade, high risk of recurrence, or poor survival. It can also have a valuable role during preoperative and preradiation planning, as well as intraoperative imaging guidance. For example, choline to NAA ratio measured by MRS can localize the site within the tumor with the highest cellularity, which can be targeted for biopsy[87,88] and gamma knife radiosurgery.[89] Applying machine learning algorithms to multiparametric MRI data, several groups have developed voxel-based models to classify glioma into tissues of different tumor grades or tumor cell density, verified by subsequent histological analysis.[90,91] MRI features extracted from tumor and peritumoral tissues have been used to build models that can identify high-risk sites for tumor recurrence.[92] Dynamic FET-PET has been shown to help stratify prognosis, with ^{18}F-FET positive gliomas with decreasing time activity curves in kinetic analysis showing shorter progression-free survival and faster malignant transformation.[93] Furthermore, FET-PET is useful in biopsy planning, with focal regions of high-grade FET kinetics or 'hot spots' on FET-PET correlating with increased diagnostic yield for stereotactic core needle biopsy and also correlating with higher tumor grade.[94]

Prediction of patient outcome prior to antiangiogenic treatment

Two phase III clinical trials have revealed no significant survival advantage when bevacizumab, an antibody targeting vascular endothelial factor (VEGF), was added to the standard treatment for patients with newly diagnosed glioblastoma.[95,96] There is a need to identify pretreatment predictive markers that can accurately identify patients who may benefit from antiangiogenic treatment.

ADC histogram analysis of MRI imaging data of recurrent glioblastoma performed prior to anti-VEGF therapy has been shown to predict response and survival based on several retrospective

studies,[97,98] as well as evaluation of imaging data from several phase II trials.[99] Pretreatment DSC-MRI has also been shown to correlate with survival outcome for patients with recurrent glioblastoma receiving bevacizumab.[100,101] Radiomic evaluations using multiparametric MRI data have identified pretreatment prognostic imaging features for overall survival.[102–106]

Response assessment and treatment monitoring

Pseudoprogression versus *true progression in glioblastomas*

Following standard-of-care upfront treatment including maximal safe resection, radiation with adjuvant temozolomide, 20–30% of patients with glioblastoma develop increased contrast enhancement within 3 months from end of radiation treatment that resolves without changes in treatment.[107] If patients with pseudoprogression were treated the same way as the true progressors, they may not continue to receive potentially beneficial adjuvant temozolomide chemotherapy and may be inappropriately included in trials of progressive/recurrent glioma.[107] To mitigate this problem, the Response Assessment in Neuro-Oncology (RANO) criteria require a minimum of 12 weeks after completion of radiation treatment before tumor progression can be confirmed unless the site of progressive disease is distant from the radiation field or there is pathologic evidence of progressive/recurrent tumor.[107] In a phase III trial of bevacizumab or placebo plus radiotherapy/temozolomide for newly diagnosed glioblastoma (AVAglio), 9.3% had confirmed pseudoprogression in the placebo arm,[108] indicating that the incidence of pseudoprogression appears lower than initially reported. Nevertheless, pseudoprogression can affect progression assessment in a small but non-negligible number of patients. In actual clinical practice, it remains a challenge to determine the true status of tumors that show early apparent progression based on conventional imaging assessment. In recent years, there have been tremendous efforts in discovering and applying advanced imaging techniques to improve the diagnosis of pseudoprogression.

Compared to normal brain tissue or necrosis, recurrent or progressive tumor more commonly demonstrates lower ADC values.[109,110] Voxel-wise analysis of ADC maps can differentiate pseudoprogression from true progression in glioblastoma using ADC parametric response maps.[111] High b-value DW-MRI appears to improve the accuracy of diagnosing pseudoprogression compared to standard DW-MRI.[112]

A number of prior studies have examined the ability of DSC-MRI to distinguish pseudoprogression from tumor progression in glioblastoma.[113–117] Compared to true tumor progression, treatment-related necrosis or pseudoprogression exhibits lower relative blood volume (Figure 2). DCE-MRI can also differentiate tumor progression from radiation necrosis,[118–120] although there is also evidence that there is no significant difference between DSC-MRI and DCE-MRI when either is added to standard MRI.[121] Parameters derived from combined approaches including DTI and DSC can classify tissues into true progressive tumor, treatment necrosis, and mixed response.[122]

Based on altered metabolite concentrations in tissues, single-voxel MRS can distinguish suspected progressive/recurrent tumor from treatment-related changes.[123–126] The overall diagnostic performance of MRS using choline to NAA ratio in differentiating glioma progression from radiation necrosis has sensitivity and specificity of 0.88 and 0.86, respectively.[127] Multivoxel MRS can evaluate spatially heterogeneous tissues containing mixtures of recurrent tumor and treatment effect.[128–133]

FDG-PET has been evaluated for its diagnostic accuracy in distinguishing delayed radiation necrosis from recurrent tumor,[134–138] although it is unclear whether these results are applicable for the cases pseudoprogression that typically occur at earlier times following chemoradiation. Due to high background uptake by the normal brain, FDG radiotracer may also not detect small recurrent lesions. Several studies have reported utility of amino acid PET, including c-methionine, F-DOPA, FET, and FLT for diagnosing tumor progression.[139–145] There is evidence of improved diagnostic accuracy comparing to FDG-PET.[139,146] For patients with glioblastoma following standard chemoradiation therapy who present with suspected progression 3 months after completion of treatment, FET-PET can diagnose pseudoprogression with sensitivity 84%, specificity 86%, and accuracy 85%.[147] More recently, texture analysis has been applied to amino acid PET imaging data with some success in defining pseudoprogression.[148]

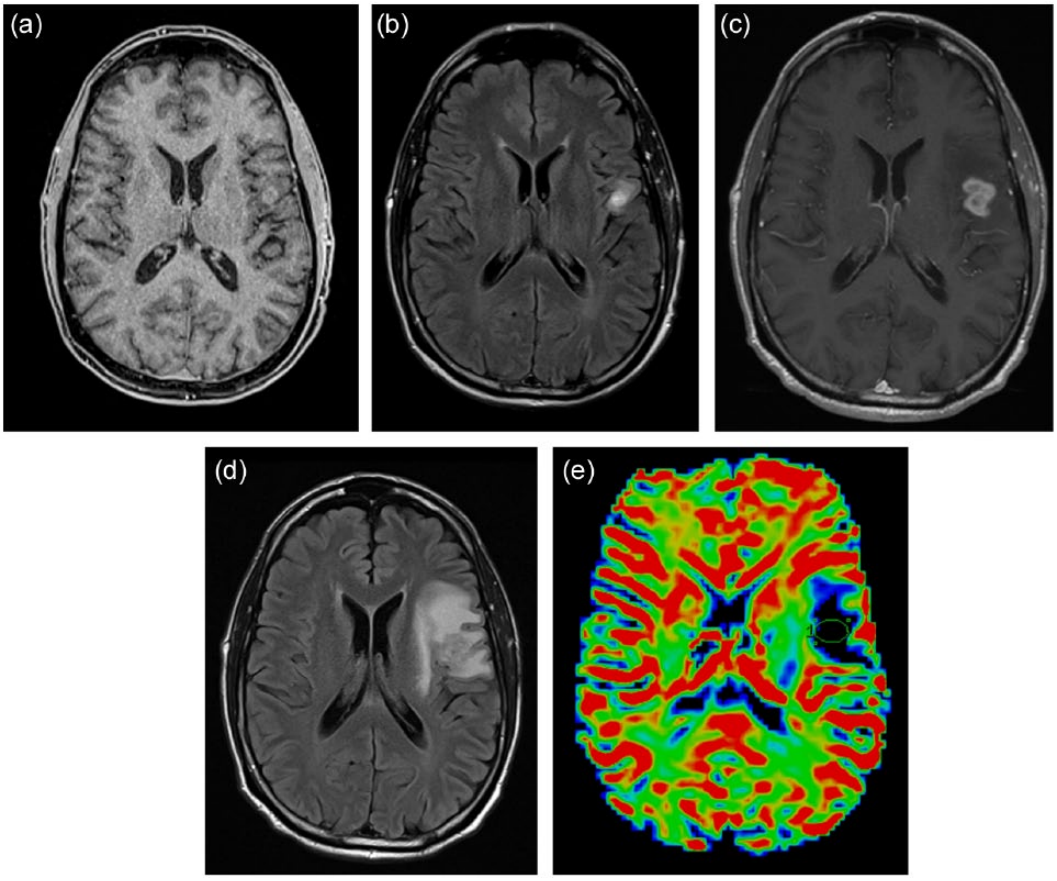

Figure 2. A 62-year-old man with glioblastoma treated by concomitant temozolomide and radiation. Axial gadolinium-enhanced T1-weighted (a) and fluid-attenuated inversion recovery (FLAIR) (b) images demonstrate a small area of enhancement in the left inferior frontal lobe after three cycles of adjuvant temozolomide treatment. At the fifth cycle of adjuvant treatment, there is increased nodular enhancement (c) and surrounding T2/FLAIR signal abnormalities (d) suspicious for progression. (e) Dynamic susceptibility contrast magnetic resonance imaging (DSC-MRI) perfusion imaging showed no evidence of elevated blood volume. Subsequent surgical resection revealed evidence of necrosis without tumor cells.

Response evaluation during antiangiogenic therapy

Antiangiogenic therapies such as bevacizumab, a humanized monoclonal antibody against VEGF and cediranib, a VEGF receptor inhibitor, can result in rapid normalization of vascular permeability, reducing the intensity of contrast enhancement on T1-weighted MRI.[107,149,150] This imaging phenomenon is not associated with improved patient survival and therefore has been described as a 'pseudoresponse'.[107,151] A subset of patients with progressive tumor can also manifest as enlarging nonenhancing T2/FLAIR abnormality on imaging.[107,151] The RANO criteria included guidelines requiring evaluation of T2/FLAIR images for determination of progression.[107] There is evidence that development of enlarging T2/FLAIR abnormality has been associated with subsequent progression of enhancing lesions.[152] A retrospective evaluation of the imaging data from the phase II BRAIN trial of bevacizumab treated recurrent glioblastoma demonstrated that the RANO criteria resulted in a small but significant difference in median progression-free survival than did the Macdonald criteria.[153] Currently, evaluation of nonenhancing tumor as defined by the RANO criteria is qualitative based on subjective review of T2/FLAIR imaging by expert readers of progression.[107] There is an urgent need for imaging strategies that can be employed as an objective surrogate in evaluating tumor burden in the setting of antiangiogenic therapy.

Nonenhancing tumor on T2/FLAIR MRI has been categorized by morphology as circumscribed *versus*

infiltrative lesions.[154] Patients with nonenhancing circumscribed T2/FLAIR had worse survival outcomes comparing to those with infiltrative nonenhancing lesions, as well as those with enhancing progressive disease following initiation of bevacizumab.[155,156] Although this approach of characterizing lesion morphology remains subjective, the qualitative imaging descriptors provide improved specificity with respect to patient outcome.[107] Volumetric methods have been proposed as an objective criteria in measuring T2/FLAIR lesions, although in the BELOB trial data obtained using such an approach did not result in improved post-treatment prognostication accuracy as compared to the RANO criteria.[157]

T1 subtraction and T2 mapping techniques have been applied to evaluating post-bevacizumab treated patients with recurrent glioblastomas.[158,159] These methods utilize commercially available MRI sequences that are commonly done for brain tumor evaluation and can be readily incorporated into the clinical workflow if postprocessing can be automated. DW-MRI is also commonly performed during routine brain tumor evaluation, and low ADC lesions observed on DW-MRI following bevacizumab treatment have been associated with progressive tumor.[160] High b-value DW-MRI improves detection of pseudoresponse over standard DW-MRI in patients treated with bevacizumab.[161] The specificity of low ADC lesions for active tumor has been questioned, since there have also been reports of hypoxic or necrotic tissue associated with these lesions.[162] Pathological analysis provides evidence that progressively expanding low ADC lesions contain coagulative necrosis surrounded by viable tumor.[163] An ADC threshold value of 0.736×10^{-3} mm^2/s has been shown to be a potential differentiating factor of hypercellular tumor and necrosis.[163] Patients with larger low-ADC volumes after bevacizumab treatment had worse overall survival.[164] Advanced DW-MRI techniques such as histogram analysis of ADC and RSI has also been shown to predict overall survival following bevacizumab treatment.[165,166] Perfusion imaging techniques including DSC-MRI and DCE-MRI also provide prognostic information during early post-bevacizumab treatment evaluation of patients with recurrent glioblastomas.[167–170] There is early evidence that amino acid PET provides greater specificity than standard MRI for evaluation of progressive tumor and provides prognosis during antiangiogenic therapy[171–173] (Figure 3). Combined-modality FMISO PET and MRI evaluated patients with recurrent high-grade glioma and revealed patterns of hypoxia after antiangiogenic therapy; enlarging nonenhancing mass showed reduced diffusion, lack of hypoxia, and preserved cerebral blood volume.[21]

Response evaluation during immunotherapy

With the advent of new and emerging immunotherapies such as cytotoxic T-lymphocyte-4 (CTLA-4) immune checkpoint molecules such as ipilumimab, and programmed cell 1 agents such as nivolumab and pembrolizumab for metastatic melanoma and non-small cell lung cancer, establishing progression has had its challenges.[174–176] Findings of classic progression including increasing size, enhancement, and edema may not reflect progression with immunotherapies that may involve a localized and temporary inflammatory response before subsequent improvement.[177] Furthermore, patterns of initial increase in target tumor size have preceded subsequent decrease in tumor size, with metastatic melanoma treated with anti-PD/PD-L1 therapy.[178,179] The Immunotherapy Response Assessment in Neuro-Oncology (iRANO) working group has sought to address this by requiring a confirmation scan at 3 months for patients who presents with enlarging enhancement within 6 months from initiation of immunotherapy (Figure 4).[180] The 6-month cutoff time was empirically determined, but presentation of pseudoprogression beyond 6 months has been reported.[181] Furthermore, the 3-month time duration until the confirmatory scan could be a challenge in clinical practice since patients are often symptomatic. While further evaluation of data from immunotherapy trials is needed to provide support for the iRANO criteria, an imaging marker allowing accurate differentiation of immunotherapy-related changes from recurrent/progressive tumor is ultimately needed to improve management of patients undergoing immunotherapy. In small case series of patients with melanoma brain metastases treated with checkpoint inhibitors, dynamic FET-PET imaging appears to correctly identify pseudoprogression,[182] highlighting the potential application for the technique in imaging of patients with high-grade glioma. Finally, PET radiotracers targeting immune response are being developed. In a syngeneic immunocompetent mice model,

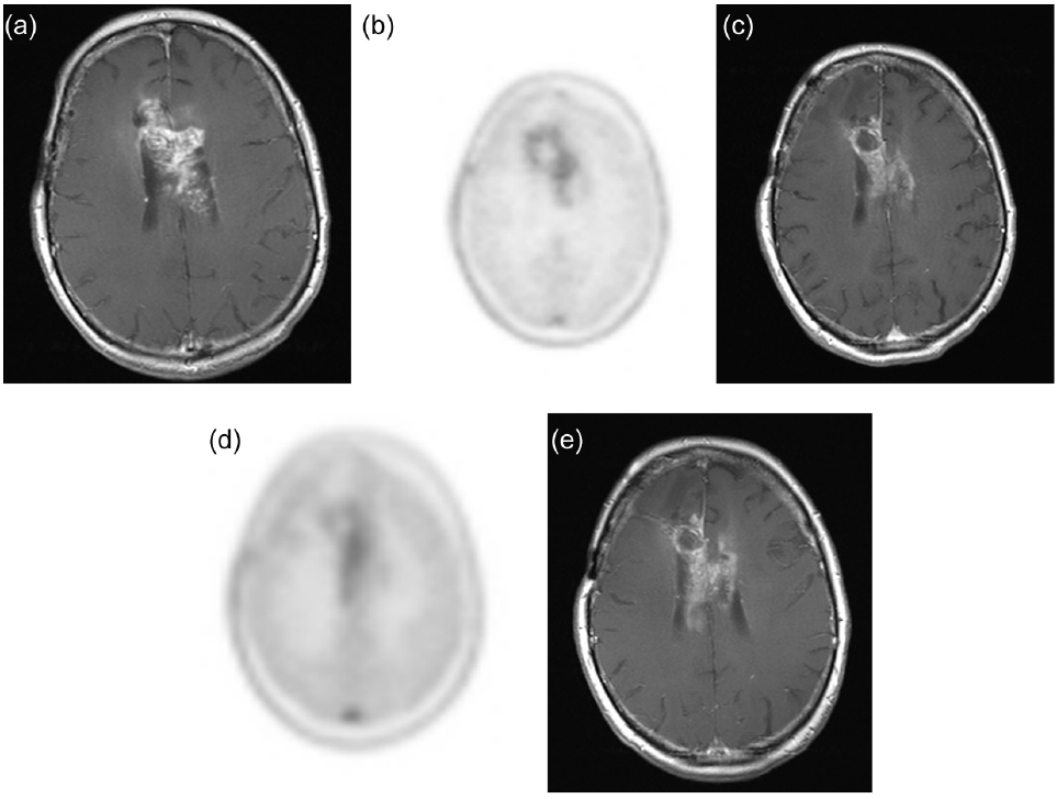

Figure 3. A 58-year-old man with recurrent glioblastoma receiving bevacizumab monotherapy. Pretreatment axial gadolinium-enhanced T1-weighted image (a) and 18F-fluoro-ethyl-tyrosine (FET) positron emission tomography image (b) showed an enhancing mass centered in the body of the corpus callosum with moderate FET avidity. After one dose of bevacizumab, the extent and intensity of enhancement both reduced as evident on the axial T1-weighted image (c), but there persists a slightly increased FET uptake in the left aspect of the mass (d). This area of abnormality showed increased enhancement on the subsequent axial gadolinium-enhanced T1-weighted image (e).

immune responses can be detected after immunotherapy in glioblastoma using PET radiotracer for deoxycytidine kinase (dCK).[183]

Challenges and outlook

While numerous novel imaging methods have been applied to address various clinical challenges faced by treating oncologists today, most of these techniques as outlined in this review still require validation from large prospective trials. Currently the acquisition protocol for evaluating brain tumors is highly variable among imaging centers, and such variability can impact the generalizability of imaging techniques across different sites. Recently, a standardized MRI protocol has been proposed specifying the acquisition parameters of conventional and diffusion MRI sequences,[184] as well as perfusion MRI.[185] Wider adoptions of these standardized protocols in the neuro-oncology community should aid the ongoing and future efforts in the discovery and validation of imaging markers in multicenter trials.

Machine learning approaches to neuro-oncologic imaging is only in its earliest phase of development and many of the results outlined in this review are not ready to be incorporated into clinical practice. For one, the current voxel-based analysis of imaging data requires whole-tumor segmentation, which has been a bottleneck in research progress and clinical implementation. This problem is currently being automated using state-of-the-art machine learning algorithms, with promising results.[186–190] Furthermore, the machine learning approach can facilitate integration of data beyond imaging, including clinical and molecular markers, making this approach integral to diagnostic, prognostic, and predictive biomarker development and implementation. It is important to note that development and validation of machine learning models require large,

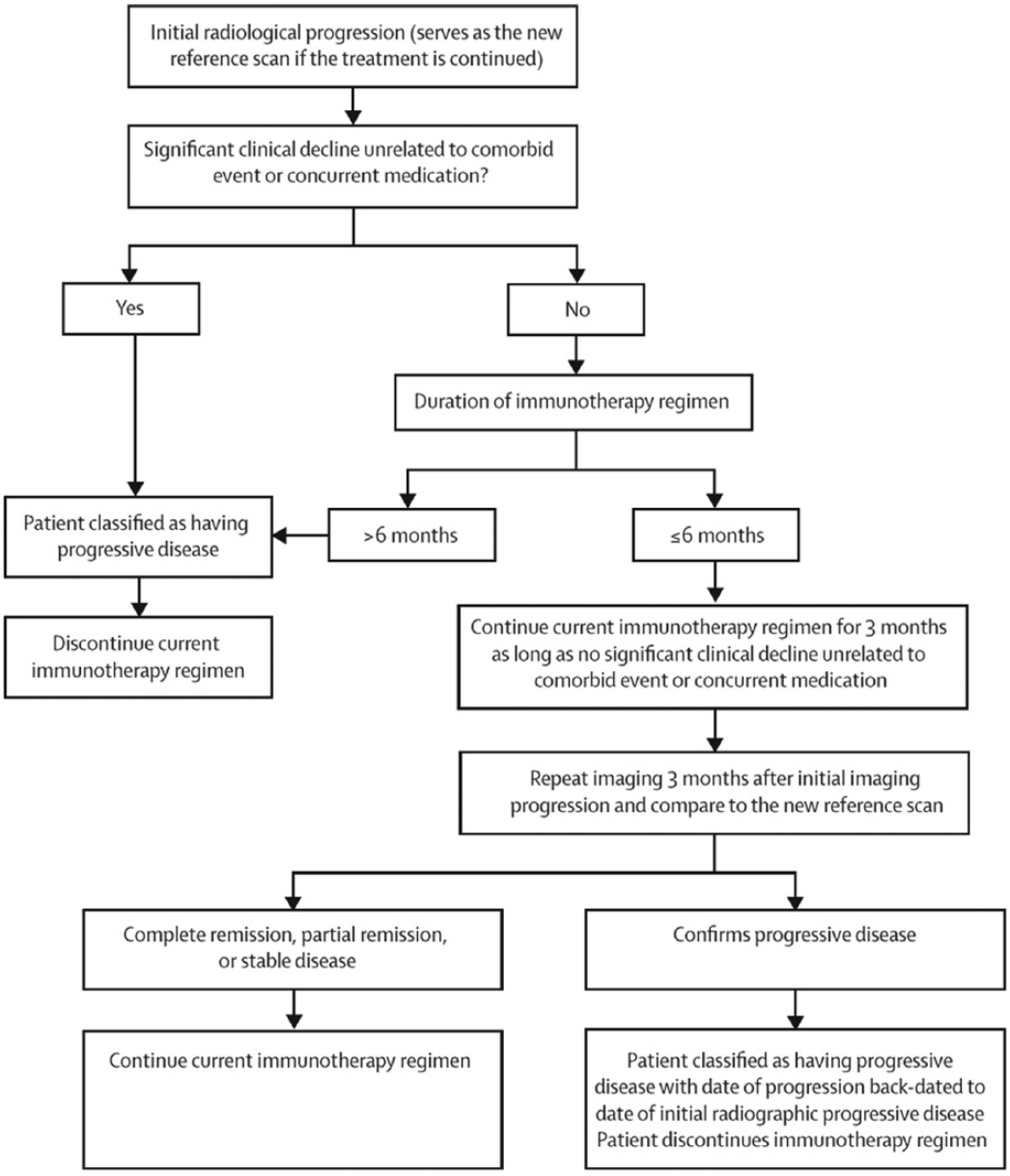

Figure 4. Schematic flowchart of the Immunotherapy Response Assessment in Neuro-Oncology criteria for response assessment in immunotherapy.
Permission to reprint from *Lancet Oncology*.

well-annotated datasets, and therefore multidisciplinary efforts and multicenter collaborations are necessary.

Conclusion

Imaging plays several key roles in managing brain tumors, including diagnosis, prognosis, and treatment response assessment. There have been important innovations in numerous advanced imaging techniques with the aim of improving the accuracy of tumor diagnosis and address challenging clinical problems, including evaluation of pseudoprogression and response to antiangiogenic therapy and immunotherapy. Some of these techniques have already been incorporated as routine tumor evaluation in large centers, while many others are currently being validated for accuracy and reproducibility. Understanding the advantages and limitations of these techniques is essential in advancing our goal of personalized care for patients with brain tumors.

Funding

This research received no specific grant from any funding agency in the public, commercial, or not-for-profit sectors.

Conflict of interest statement

The authors declare that there is no conflict of interest.

References

1. Hayashida Y, Hirai T, Morishita S, *et al*. Diffusion-weighted imaging of metastatic brain tumors: comparison with histologic type and tumor cellularity. *AJNR Am J Neuroradiol* 2006; 27: 1419–1425.
2. Seo HS, Chang KH, Na DG, *et al*. High b-value diffusion (b = 3000 s/mm^2) MR imaging in cerebral gliomas at 3T: visual and quantitative comparisons with b = 1000 s/mm^2. *Am J Neuroradiol* 2008; 29: 458–463.
3. Hui ES, Cheung MM, Qi L, *et al*. Towards better MR characterization of neural tissues using directional diffusion kurtosis analysis. *NeuroImage* 2008; 42: 122–134.
4. Ellingson BM, Sahebjam S, Kim HJ, *et al*. Pretreatment ADC histogram analysis is a predictive imaging biomarker for bevacizumab treatment but not chemotherapy in recurrent glioblastoma. *AJNR Am J Neuroradiol* 2014; 35: 673–679.
5. Ellingson BM, Cloughesy TF, Zaw T, *et al*. Functional diffusion maps (fDMs) evaluated before and after radiochemotherapy predict progression-free and overall survival in newly diagnosed glioblastoma. *Neuro-Oncol* 2012; 14: 333–343.
6. Krishnan AP, Karunamuni R, Leyden KM, *et al*. Restriction spectrum imaging improves risk stratification in patients with glioblastoma. *AJNR Am J Neuroradiol* 2017; 38: 882–889.
7. Wang S, Kim SJ, Poptani H, *et al*. Diagnostic utility of diffusion tensor imaging in differentiating glioblastomas from brain metastases. *AJNR Am J Neuroradiol* 2014; 35: 928–934.
8. Rosen BR, Belliveau JW, Vevea JM, *et al*. Perfusion imaging with NMR contrast agents. *Magn Reson Med* 1990; 14: 249–265.
9. Villringer A, Rosen BR, Belliveau JW, *et al*. Dynamic imaging with lanthanide chelates in normal brain: contrast due to magnetic susceptibility effects. *Magn Reson Med* 1988; 6: 164–174.
10. Tofts PS and Kermode AG. Measurement of the blood–brain barrier permeability and leakage space using dynamic MR imaging: 1. Fundamental concepts. *Magn Reson Med* 1991; 17: 357–367.
11. Tofts PS. Modeling tracer kinetics in dynamic Gd-DTPA MR imaging. *J Magn Reson Imaging JMRI* 1997; 7: 91–101.
12. Tofts PS, Brix G, Buckley DL, *et al*. Estimating kinetic parameters from dynamic contrast-enhanced T(1)-weighted MRI of a diffusable tracer: standardized quantities and symbols. *J Magn Reson Imaging JMRI* 1999; 10: 223–232.
13. Hu LS, Kelm Z, Korfiatis P, *et al*. Impact of software modeling on the accuracy of perfusion MRI in glioma. *AJNR Am J Neuroradiol* 2015; 36: 2242–2249.
14. Oz G, Alger JR, Barker PB, *et al*. Clinical proton MR spectroscopy in central nervous system disorders. *Radiology* 2014; 270: 658–679.
15. Kelloff GJ, Hoffman JM, Johnson B, *et al*. Progress and promise of FDG-PET imaging for cancer patient management and oncologic drug development. *Clin Cancer Res* 2005; 11: 2785–2808.
16. Di Chiro G, DeLaPaz RL, Brooks RA, *et al*. Glucose utilization of cerebral gliomas measured by [18F] fluorodeoxyglucose and positron emission tomography. *Neurology* 1982; 32: 1323–1329.
17. Isselbacher KJ. Sugar and amino acid transport by cells in culture: differences between normal and malignant cells. *N Engl J Med* 1972; 286: 929–933.
18. Busch H, Davis JR, Honig GR, *et al*. The uptake of a variety of amino acids into nuclear proteins of tumors and other tissues. *Cancer Res* 1959; 19: 1030–1039.
19. Kato T, Shinoda J, Oka N, *et al*. Analysis of ^{11}C-methionine uptake in low-grade gliomas and correlation with proliferative activity. *AJNR Am J Neuroradiol* 2008; 29: 1867–1871.
20. Sato N, Suzuki M, Kuwata N, *et al*. Evaluation of the malignancy of glioma using ^{11}C-methionine positron emission tomography and proliferating cell nuclear antigen staining. *Neurosurg Rev* 1999; 22: 210–214.
21. Barajas RF, Krohn KA, Link JM, *et al*. Glioma FMISO PET/MR imaging concurrent with antiangiogenic therapy: molecular imaging

as a clinical tool in the burgeoning era of personalized medicine. *Biomedicines* 2016; 4: E24.

22. Gerstner ER, Zhang Z, Fink JR, *et al*. ACRIN 6684: assessment of tumor hypoxia in newly diagnosed glioblastoma using 18F-FMISO PET and MRI. *Clin Cancer Res* 2016; 22: 5079–5086.
23. Kumar V, Gu Y, Basu S, *et al*. Radiomics: the process and the challenges. *Magn Reson Imaging* 2012; 30: 1234–1248.
24. Lambin P, Rios-Velazquez E, Leijenaar R, *et al*. Radiomics: extracting more information from medical images using advanced feature analysis. *Eur J Cancer* 2012; 48: 441–446.
25. Lee J, Narang S, Martinez JJ, *et al*. Associating spatial diversity features of radiologically defined tumor habitats with epidermal growth factor receptor driver status and 12-month survival in glioblastoma: methods and preliminary investigation. *J Med Imaging Bellingham* 2015; 2: 041006.
26. Huang YQ, Liang CH, He L, *et al*. Development and validation of a radiomics nomogram for preoperative prediction of lymph node metastasis in colorectal cancer. *J Clin Oncol* 2016; 34: 2157–2164.
27. Guo W, Li H, Zhu Y, *et al*. Prediction of clinical phenotypes in invasive breast carcinomas from the integration of radiomics and genomics data. *J Med Imaging Bellingham* 2015; 2: 041007.
28. Giesel F, Schneider F, Kratochwil C, *et al*. CT radiomic analysis using lymph-node-density profile in correlation to SUV-value for PET/CT based N-staging. *J Nucl Med* 2017; 58(2): 282–287.
29. Guo AC, Cummings TJ, Dash RC, *et al*. Lymphomas and high-grade astrocytomas: comparison of water diffusibility and histologic characteristics. *Radiology* 2002; 224: 177–183.
30. Stadnik TW, Chaskis C, Michotte A, *et al*. Diffusion-weighted MR imaging of intracerebral masses: comparison with conventional MR imaging and histologic findings. *AJNR Am J Neuroradiol* 2001; 22: 969–976.
31. Toh CH, Castillo M, Wong AMC, *et al*. Primary cerebral lymphoma and glioblastoma multiforme: differences in diffusion characteristics evaluated with diffusion tensor imaging. *AJNR Am J Neuroradiol* 2008; 29: 471–475.
32. Wang S, Kim S, Chawla S, *et al*. Differentiation between glioblastomas, solitary brain metastases, and primary cerebral lymphomas using diffusion tensor and dynamic susceptibility contrast-enhanced MR imaging. *AJNR Am J Neuroradiol* 2011; 32: 507–514.
33. Lu S, Gao Q, Yu J, *et al*. Utility of dynamic contrast-enhanced magnetic resonance imaging for differentiating glioblastoma, primary central nervous system lymphoma and brain metastatic tumor. *Eur J Radiol* 2016; 85: 1722–1727.
34. Lin X, Lee M, Buck O, *et al*. Diagnostic accuracy of T1-weighted dynamic contrast-enhanced-MRI and DWI-ADC for differentiation of glioblastoma and primary CNS lymphoma. *AJNR Am J Neuroradiol* 2017; 38: 485–491.
35. Radbruch A, Wiestler B, Kramp L, *et al*. Differentiation of glioblastoma and primary CNS lymphomas using susceptibility weighted imaging. *Eur J Radiol* 2013; 82: 552–556.
36. Kunimatsu A, Kunimatsu N, Kamiya K, *et al*. Comparison between glioblastoma and primary central nervous system lymphoma using MR image-based texture analysis. *Magn Reson Med Sci* 2018; 17: 50–57.
37. Caravan I, Ciortea CA, Contis A, *et al*. Diagnostic value of apparent diffusion coefficient in differentiating between high-grade gliomas and brain metastases. *Acta Radiol* 2017. Epub ahead of print January 2017. DOI: 10.1177/0284185117727787.
38. Lee EJ, terBrugge K, Mikulis D, *et al*. Diagnostic value of peritumoral minimum apparent diffusion coefficient for differentiation of glioblastoma multiforme from solitary metastatic lesions. *AJR Am J Roentgenol* 2011; 196: 71–76.
39. Eidel O, Burth S, Neumann JO, *et al*. Tumor infiltration in enhancing and non-enhancing parts of glioblastoma: a correlation with histopathology. *PLoS One* 2017; 12: e0169292.
40. Chawla S, Zhang Y, Wang S, *et al*. Proton magnetic resonance spectroscopy in differentiating glioblastomas from primary cerebral lymphomas and brain metastases. *J Comput Assist Tomogr* 2010; 34: 836–841.
41. Wijnen JP, Idema AJS, Stawicki M, *et al*. Quantitative short echo time 1H MRSI of the peripheral edematous region of human brain tumors in the differentiation between glioblastoma, metastasis, and meningioma. *J Magn Reson Imaging JMRI* 2012; 36: 1072–1082.
42. Ma JH, Kim HS, Rim NJ, *et al*. Differentiation among glioblastoma multiforme, solitary metastatic tumor, and lymphoma using whole-tumor histogram analysis of the normalized

cerebral blood volume in enhancing and perienhancing lesions. *AJNR Am J Neuroradiol* 2010; 31: 1699–1706.

43. Stadlbauer A, Moser E, Gruber S, *et al.* Improved delineation of brain tumors: an automated method for segmentation based on pathologic changes of 1H-MRSI metabolites in gliomas. *NeuroImage* 2004; 23: 454–461.

44. Pamir MN, Ozduman K, Dinçer A, *et al.* First intraoperative, shared-resource, ultrahigh-field 3-Tesla magnetic resonance imaging system and its application in low-grade glioma resection. *J Neurosurg* 2010; 112: 57–69.

45. Louis DN, Perry A, Reifenberger G, *et al.* The 2016 World Health Organization classification of tumors of the central nervous system: a summary. *Acta Neuropathol (Berl)* 2016; 131: 803–820.

46. Macyszyn L, Akbari H, Pisapia JM, *et al.* Imaging patterns predict patient survival and molecular subtype in glioblastoma via machine learning techniques. *Neuro-Oncol* 2016; 18: 417–425.

47. Korfiatis P, Kline TL, Coufalova L, *et al.* MRI texture features as biomarkers to predict MGMT methylation status in glioblastomas. *Med Phys* 2016; 43: 2835.

48. Xi YB, Guo F, Xu ZL, *et al.* Radiomics signature: a potential biomarker for the prediction of MGMT promoter methylation in glioblastoma. *J Magn Reson Imaging JMRI.* Epub ahead of print 2017. DOI: 10.1002/jmri.25860.

49. Kickingereder P, Bonekamp D, Nowosielski M, et al. Radiogenomics of glioblastoma: machine learning-based classification of molecular characteristics by using multiparametric and multiregional MR imaging features. *Radiology* 2016; 281: 907–918.

50. Bakas S, Akbari H, Pisapia J, *et al.* In vivo detection of EGFRvIII in glioblastoma via perfusion magnetic resonance imaging signature consistent with deep peritumoral infiltration: the ϕ-index. *Clin Cancer Res* 2017; 23: 4724–4734.

51. Andronesi OC, Rapalino O, Gerstner E, *et al.* Detection of oncogenic IDH1 mutations using magnetic resonance spectroscopy of 2-hydroxyglutarate. *J Clin Invest* 2013; 123: 3659–3663.

52. Andronesi OC, Loebel F, Bogner W, *et al.* Treatment response assessment in IDH-mutant glioma patients by non-invasive 3D functional spectroscopic mapping of 2-hydroxyglutarate. *Clin Cancer Res* 2016; 22: 1632–1641.

53. Choi C, Raisanen JM, Ganji SK, *et al.* Prospective longitudinal analysis of 2-hydroxyglutarate magnetic resonance spectroscopy identifies broad clinical utility for the management of patients with IDH-mutant glioma. *J Clin Oncol* 2016; 34: 4030–4039.

54. Verger A, Stoffels G, Bauer EK, *et al.* Static and dynamic 18F-FET PET for the characterization of gliomas defined by IDH and 1p/19q status. *Eur J Nucl Med Mol Imaging* 2018; 45: 443–451.

55. Zhang B, Chang K, Ramkissoon S, *et al.* Multimodal MRI features predict isocitrate dehydrogenase genotype in high-grade gliomas. *Neuro-Oncol* 2017; 19: 109–117.

56. Zhou H, Vallières M, Bai HX, *et al.* MRI features predict survival and molecular markers in diffuse lower-grade gliomas. *Neuro-Oncol* 2017; 19: 862–870.

57. Stadlbauer A, Zimmermann M, Kitzwögerer M, *et al.* MR imaging-derived oxygen metabolism and neovascularization characterization for grading and IDH gene mutation detection of gliomas. *Radiology* 2017; 283: 799–809.

58. Ostrom QT, Gittleman H, Liao P, *et al.* CBTRUS statistical report: primary brain and central nervous system tumors diagnosed in the United States in 2007–2011. *Neuro-Oncol* 2014; 16(Suppl. 4): iv1–iv63.

59. Rutten EH, Doesburg WH and Slooff JL. Histologic factors in the grading and prognosis of astrocytoma grade I–IV. *J Neurooncol* 1992; 13: 223–230.

60. Al-Okaili RN, Krejza J, Woo JH, *et al.* Intraaxial brain masses: MR imaging-based diagnostic strategy – initial experience. *Radiology* 2007; 243: 539–550.

61. García-Gómez JM, Luts J, Julià-Sapé M, *et al.* Multiproject-multicenter evaluation of automatic brain tumor classification by magnetic resonance spectroscopy. *MAGMA* 2009; 22: 5–18.

62. Vicente J, Fuster-Garcia E, Tortajada S, *et al.* Accurate classification of childhood brain tumours by in vivo ^{1}H MRS: a multi-centre study. *Eur J Cancer* 2013; 49: 658–667.

63. Tate AR, Underwood J, Acosta DM, *et al.* Development of a decision support system for diagnosis and grading of brain tumours using in vivo magnetic resonance single voxel spectra. *NMR Biomed* 2006; 19: 411–434.

64. Julià-Sapé M, Coronel I, Majós C, *et al*. Prospective diagnostic performance evaluation of single-voxel 1H MRS for typing and grading of brain tumours. *NMR Biomed* 2012; 25: 661–673.

65. Morita N, Wang S, Chawla S, *et al*. Dynamic susceptibility contrast perfusion weighted imaging in grading of nonenhancing astrocytomas. *J Magn Reson Imaging* 2010; 32: 803–808.

66. Shiroishi MS, Castellazzi G, Boxerman JL, *et al*. Principles of T2*-weighted dynamic susceptibility contrast MRI technique in brain tumor imaging. *J Magn Reson Imaging* 2015; 41: 296–313.

67. Kincaid PK, El-Saden SM, Park SH, *et al*. Cerebral ganglioglomas: preoperative grading using FDG-PET and 201Tl-SPECT. *AJNR Am J Neuroradiol* 1998; 19: 801–806.

68. Delbeke D, Meyerowitz C, Lapidus RL, *et al*. Optimal cutoff levels of F-18 fluorodeoxyglucose uptake in the differentiation of low-grade from high-grade brain tumors with PET. *Radiology* 1995; 195: 47–52.

69. Collet S, Valable S, Constans JM, *et al*. [(18) F]-fluoro-L-thymidine PET and advanced MRI for preoperative grading of gliomas. *NeuroImage Clin* 2015; 8: 448–454.

70. Jansen NL, Suchorska B, Wenter V, *et al*. Prognostic significance of dynamic 18F-FET PET in newly diagnosed astrocytic high-grade glioma. *J Nucl Med* 2015; 56: 9–15.

71. Suchorska B, Giese A, Biczok A, *et al*. Identification of time-to-peak on dynamic 18F-FET-PET as a prognostic marker specifically in IDH1/2 mutant diffuse astrocytoma. *Neuro-Oncol* 2018; 20: 279–288.

72. Wiestler B, Kluge A, Lukas M, *et al*. Multiparametric MRI-based differentiation of WHO grade II/III glioma and WHO grade IV glioblastoma. *Sci Rep* 2016; 6: 35142.

73. Cao Y, Shen Z, Chenevert TL, *et al*. Estimate of vascular permeability and cerebral blood volume using Gd-DTPA contrast enhancement and dynamic T2*-weighted MRI. *J Magn Reson Imaging* 2006; 24: 288–296.

74. Hu LS, Eschbacher JM, Dueck AC, *et al*. Correlations between perfusion MR imaging cerebral blood volume, microvessel quantification, and clinical outcome using stereotactic analysis in recurrent high-grade glioma. *Am J Neuroradiol* 2012; 33: 69–76.

75. Jain R, Poisson LM, Gutman D, *et al*. Outcome prediction in patients with glioblastoma by using imaging, clinical, and genomic biomarkers: focus on the nonenhancing component of the tumor. *Radiology* 2014; 272: 484–493.

76. Kim R, Choi SH, Yun TJ, *et al*. Prognosis prediction of non-enhancing T2 high signal intensity lesions in glioblastoma patients after standard treatment: application of dynamic contrast-enhanced MR imaging. *Eur Radiol* 2017; 27: 1176–1185.

77. Han H, Han C, Wu X, *et al*. Preoperative grading of supratentorial nonenhancing gliomas by high b-value diffusion-weighted 3T magnetic resonance imaging. *J Neurooncol* 2017; 133: 147–154.

78. Boonzaier NR, Larkin TJ, Matys T, *et al*. Multiparametric MR imaging of diffusion and perfusion in contrast-enhancing and nonenhancing components in patients with glioblastoma. *Radiology* 2017; 284: 180–190.

79. Prasanna P, Patel J, Partovi S, *et al*. Radiomic features from the peritumoral brain parenchyma on treatment-naïve multi-parametric MR imaging predict long versus short-term survival in glioblastoma multiforme: preliminary findings. *Eur Radiol* 2017; 27: 4188–4197.

80. Czarnek N, Clark K, Peters KB, *et al*. Algorithmic three-dimensional analysis of tumor shape in MRI improves prognosis of survival in glioblastoma: a multi-institutional study. *J Neurooncol* 2017; 132: 55–62.

81. Kickingereder P, Burth S, Wick A, *et al*. Radiomic profiling of glioblastoma: identifying an imaging predictor of patient survival with improved performance over established clinical and radiologic risk models. *Radiology* 2016; 280: 880–889.

82. Zhang Y, Li A, Peng C, *et al*. Improve glioblastoma multiforme prognosis prediction by using feature selection and multiple kernel learning. *IEEE/ACM Trans Comput Biol Bioinform* 2016; 13: 825–835.

83. Wangaryattawanich P, Hatami M, Wang J, *et al*. Multicenter imaging outcomes study of The Cancer Genome Atlas glioblastoma patient cohort: imaging predictors of overall and progression-free survival. *Neuro-Oncol* 2015; 17: 1525–1537.

84. Zhou M, Chaudhury B, Hall LO, *et al*. Identifying spatial imaging biomarkers of glioblastoma multiforme for survival group

prediction. *J Magn Reson Imaging* 2017; 46: 115–123.

85. Zinn PO, Singh SK, Kotrotsou A, *et al.* 139 Clinically applicable and biologically validated MRI radiomic test method predicts glioblastoma genomic landscape and survival. *Neurosurgery* 2016; 63(Suppl. 1): 156–157.
86. Jain R, Poisson L, Narang J, *et al.* Genomic mapping and survival prediction in glioblastoma: molecular subclassification strengthened by hemodynamic imaging biomarkers. *Radiology* 2013; 267: 212–220.
87. McKnight TR, Lamborn KR, Love TD, *et al.* Correlation of magnetic resonance spectroscopic and growth characteristics within grades II and III gliomas. *J Neurosurg* 2007; 106: 660–666.
88. Chang SM, Nelson S, Vandenberg S, *et al.* Integration of preoperative anatomic and metabolic physiologic imaging of newly diagnosed glioma. *J Neurooncol* 2009; 92: 401–415.
89. Einstein DB, Wessels B, Bangert B, *et al.* Phase II trial of radiosurgery to magnetic resonance spectroscopy-defined high-risk tumor volumes in patients with glioblastoma multiforme. *Int J Radiat Oncol Biol Phys* 2012; 84: 668–674.
90. Inano R, Oishi N, Kunieda T, *et al.* Visualization of heterogeneity and regional grading of gliomas by multiple features using magnetic resonance-based clustered images. *Sci Rep* 2016; 6: 30344.
91. Hu LS, Ning S, Eschbacher JM, *et al.* Multi-parametric MRI and texture analysis to visualize spatial histologic heterogeneity and tumor extent in glioblastoma. *PLoS One* 2015; 10: e0141506.
92. Akbari H, Macyszyn L, Da X, *et al.* Imaging surrogates of infiltration obtained via multiparametric imaging pattern analysis predict subsequent location of recurrence of glioblastoma. *Neurosurgery* 2016; 78: 572–580.
93. Jansen NL, Suchorska B, Wenter V, *et al.* Dynamic 18F-FET PET in newly diagnosed astrocytic low-grade glioma identifies high-risk patients. *J Nucl Med* 2014; 55: 198–203.
94. Kunz M, Thon N, Eigenbrod S, *et al.* Hot spots in dynamic (18)FET-PET delineate malignant tumor parts within suspected WHO grade II gliomas. *Neuro-Oncol* 2011; 13: 307–316.
95. Chinot OL, Wick W, Mason W, *et al.* Bevacizumab plus radiotherapy-temozolomide for newly diagnosed glioblastoma. *N Engl J Med* 2014; 370: 709–722.
96. Gilbert MR, Dignam JJ, Armstrong TS, *et al.* A randomized trial of bevacizumab for newly diagnosed glioblastoma. *N Engl J Med* 2014; 370: 699–708.
97. Rahman R, Hamdan A, Zweifler R, *et al.* Histogram analysis of apparent diffusion coefficient within enhancing and nonenhancing tumor volumes in recurrent glioblastoma patients treated with bevacizumab. *J Neurooncol* 2014; 119: 149–158.
98. Pope WB, Kim HJ, Huo J, *et al.* Recurrent glioblastoma multiforme: ADC histogram analysis predicts response to bevacizumab treatment. *Radiology* 2009; 252: 182–189.
99. Ellingson BM, Gerstner ER, Smits M, *et al.* Diffusion MRI phenotypes predict overall survival benefit from anti-VEGF monotherapy in recurrent glioblastoma: converging evidence from phase II trials. *Clin Cancer Res* 2017; 23: 5745–5756.
100. Schmainda KM, Prah M, Connelly J, *et al.* Dynamic-susceptibility contrast agent MRI measures of relative cerebral blood volume predict response to bevacizumab in recurrent high-grade glioma. *Neuro-Oncol* 2014; 16: 880–888.
101. Kickingereder P, Radbruch A, Burth S, *et al.* MR perfusion-derived hemodynamic parametric response mapping of bevacizumab efficacy in recurrent glioblastoma. *Radiology* 2016; 279: 542–552.
102. Kickingereder P, Götz M, Muschelli J, *et al.* Large-scale radiomic profiling of recurrent glioblastoma identifies an imaging predictor for stratifying anti-angiogenic treatment response. *Clin Cancer Res* 2016; 22: 5765–5771.
103. Chang K, Zhang B, Guo X, *et al.* Multimodal imaging patterns predict survival in recurrent glioblastoma patients treated with bevacizumab. *Neuro-Oncol* 2016; 18: 1680–1687.
104. Grossmann P, Narayan V, Chang K, *et al.* Quantitative imaging biomarkers for risk stratification of patients with recurrent glioblastoma treated with bevacizumab. *Neuro-Oncol* 2017; 19: 1688–1697.
105. Kickingereder P, Götz M, Muschelli J, *et al.* Large-scale radiomic profiling of recurrent glioblastoma identifies an imaging predictor for stratifying anti-angiogenic treatment response. *Clin Cancer Res* 2016; 22: 5765–5771.
106. Liu TT, Achrol AS, Mitchell LA, *et al.* Magnetic resonance perfusion image features

uncover an angiogenic subgroup of glioblastoma patients with poor survival and better response to antiangiogenic treatment. *Neuro-Oncol* 2017; 19: 997–1007.

107. Wen PY, Macdonald DR, Reardon DA, *et al.* Updated response assessment criteria for high-grade gliomas: response assessment in neuro-oncology working group. *J Clin Oncol* 2010; 28: 1963–1972.

108. Wick W, Chinot OL, Bendszus M, *et al.* Evaluation of pseudoprogression rates and tumor progression patterns in a phase III trial of bevacizumab plus radiotherapy/temozolomide for newly diagnosed glioblastoma. *Neuro-Oncol* 2016; 18: 1434–1441.

109. Hein PA, Eskey CJ, Dunn JF, *et al.* Diffusion-weighted imaging in the follow-up of treated high-grade gliomas: tumor recurrence versus radiation injury. *AJNR Am J Neuroradiol* 2004; 25: 201–209.

110. Yoo RE, Choi SH, Kim TM, *et al.* Independent poor prognostic factors for true progression after radiation therapy and concomitant temozolomide in patients with glioblastoma: subependymal enhancement and low ADC value. *AJNR Am J Neuroradiol* 2015; 36: 1846–1852.

111. Reimer C, Deike K, Graf M, *et al.* Differentiation of pseudoprogression and real progression in glioblastoma using ADC parametric response maps. *PLoS One* 2017; 12: e0174620.

112. Chu HH, Choi SH, Ryoo I, *et al.* Differentiation of true progression from pseudoprogression in glioblastoma treated with radiation therapy and concomitant temozolomide: comparison study of standard and high-b-value diffusion-weighted imaging. *Radiology* 2013; 269: 831–840.

113. Jain R, Scarpace L, Ellika S, *et al.* First-pass perfusion computed tomography: initial experience in differentiating recurrent brain tumors from radiation effects and radiation necrosis. *Neurosurgery* 2007; 61: 778–786; discussion 786–787.

114. Barajas RF, Chang JS, Segal MR, *et al.* Differentiation of recurrent glioblastoma multiforme from radiation necrosis after external beam radiation therapy with dynamic susceptibility-weighted contrast-enhanced perfusion MR imaging. *Radiology* 2009; 253: 486–496.

115. Hu LS, Baxter LC, Smith KA, *et al.* Relative cerebral blood volume values to differentiate high-grade glioma recurrence from posttreatment radiation effect: direct correlation between image-guided tissue histopathology and localized dynamic susceptibility-weighted contrast-enhanced perfusion MR imaging measurements. *AJNR Am J Neuroradiol* 2009; 30: 552–558.

116. Matsusue E, Fink JR, Rockhill JK, *et al.* Distinction between glioma progression and post-radiation change by combined physiologic MR imaging. *Neuroradiology* 2010; 52: 297–306.

117. Sugahara T, Korogi Y, Tomiguchi S, *et al.* Posttherapeutic intraaxial brain tumor: the value of perfusion-sensitive contrast-enhanced MR imaging for differentiating tumor recurrence from nonneoplastic contrast-enhancing tissue. *AJNR Am J Neuroradiol* 2000; 21: 901–909.

118. Larsen VA, Simonsen HJ, Law I, *et al.* Evaluation of dynamic contrast-enhanced T1-weighted perfusion MRI in the differentiation of tumor recurrence from radiation necrosis. *Neuroradiology* 2013; 55: 361–369.

119. Bisdas S, Naegele T, Ritz R, *et al.* Distinguishing recurrent high-grade gliomas from radiation injury: a pilot study using dynamic contrast-enhanced MR imaging. *Acad Radiol* 2011; 18: 575–583.

120. Yoo RE, Choi SH, Kim TM, *et al.* Dynamic contrast-enhanced MR imaging in predicting progression of enhancing lesions persisting after standard treatment in glioblastoma patients: a prospective study. *Eur Radiol* 2017; 27: 3156–3166.

121. Kim HS, Ju Goh M, Kim N, *et al.* Which combination of MR imaging modalities is best for predicting recurrent glioblastoma? Study of diagnostic accuracy and reproducibility. *Radiology* 2014; 273: 831–843.

122. Wang W, Steward CE and Desmond PM. Diffusion tensor imaging in glioblastoma multiforme and brain metastases: the role of p, q, L, and fractional anisotropy. *AJNR Am J Neuroradiol* 2009; 30: 203–208.

123. Schlemmer HP, Bachert P, Herfarth KK, *et al.* Proton MR spectroscopic evaluation of suspicious brain lesions after stereotactic radiotherapy. *AJNR Am J Neuroradiol* 2001; 22: 1316–1324.

124. Dowling C, Bollen AW, Noworolski SM, *et al.* Preoperative proton MR spectroscopic imaging of brain tumors: correlation with histopathologic analysis of resection specimens. *AJNR Am J Neuroradiol* 2001; 22: 604–612.

125. Rabinov JD, Lee PL, Barker FG, *et al.* In vivo 3-T MR spectroscopy in the distinction of

recurrent glioma versus radiation effects: initial experience. *Radiology* 2002; 225: 871–879.

126. Prat R, Galeano I, Lucas A, *et al.* Relative value of magnetic resonance spectroscopy, magnetic resonance perfusion, and 2-(18F) fluoro-2-deoxy-D-glucose positron emission tomography for detection of recurrence or grade increase in gliomas. *J Clin Neurosci* 2010; 17: 50–53.

127. Zhang H, Ma L, Wang Q, *et al.* Role of magnetic resonance spectroscopy for the differentiation of recurrent glioma from radiation necrosis: a systematic review and meta-analysis. *Eur J Radiol* 2014; 83: 2181–2189.

128. McKnight TR, von dem Bussche MH, Vigneron DB, *et al.* Histopathological validation of a three-dimensional magnetic resonance spectroscopy index as a predictor of tumor presence. *J Neurosurg* 2002; 97: 794–802.

129. Yang I, Huh NG, Smith ZA, *et al.* Distinguishing glioma recurrence from treatment effect after radiochemotherapy and immunotherapy. *Neurosurg Clin N Am* 2010; 21: 181–186.

130. Rock JP, Scarpace L, Hearshen D, *et al.* Associations among magnetic resonance spectroscopy, apparent diffusion coefficients, and image-guided histopathology with special attention to radiation necrosis. *Neurosurgery* 2004; 54: 1111–1117; discussion 1117–1119.

131. Weybright P, Sundgren PC, Maly P, *et al.* Differentiation between brain tumor recurrence and radiation injury using MR spectroscopy. *AJR Am J Roentgenol* 2005; 185: 1471–1476.

132. Zeng QS, Li CF, Zhang K, *et al.* Multivoxel 3D proton MR spectroscopy in the distinction of recurrent glioma from radiation injury. *J Neurooncol* 2007; 84: 63–69.

133. Smith EA, Carlos RC, Junck LR, *et al.* Developing a clinical decision model: MR spectroscopy to differentiate between recurrent tumor and radiation change in patients with new contrast-enhancing lesions. *AJR Am J Roentgenol* 2009; 192: W45–W52.

134. Kim YH, Oh SW, Lim YJ, *et al.* Differentiating radiation necrosis from tumor recurrence in high-grade gliomas: assessing the efficacy of 18F-FDG PET, ^{11}C-methionine PET and perfusion MRI. *Clin Neurol Neurosurg* 2010; 112: 758–765.

135. Gómez-Río M, Rodríguez-Fernández A, Ramos-Font C, *et al.* Diagnostic accuracy of 201Thallium-SPECT and 18F-FDG-PET in the clinical assessment of glioma recurrence. *Eur J Nucl Med Mol Imaging* 2008; 35: 966–975.

136. Ricci PE, Karis JP, Heiserman JE, *et al.* Differentiating recurrent tumor from radiation necrosis: time for re-evaluation of positron emission tomography? *AJNR Am J Neuroradiol* 1998; 19: 407–413.

137. Di Chiro G, Oldfield E, Wright DC, *et al.* Cerebral necrosis after radiotherapy and/or intraarterial chemotherapy for brain tumors: PET and neuropathologic studies. *AJR Am J Roentgenol* 1988; 150: 189–197.

138. Valk PE, Budinger TF, Levin VA, *et al.* PET of malignant cerebral tumors after interstitial brachytherapy: demonstration of metabolic activity and correlation with clinical outcome. *J Neurosurg* 1988; 69: 830–838.

139. Chung JK, Kim YK, Kim S, *et al.* Usefulness of ^{11}C-methionine PET in the evaluation of brain lesions that are hypo- or isometabolic on 18F-FDG PET. *Eur J Nucl Med Mol Imaging* 2002; 29: 176–182.

140. Li DL, Xu YK, Wang QS, *et al.* ^{11}C-methionine and ^{18}F-fluorodeoxyglucose positron emission tomography/CT in the evaluation of patients with suspected primary and residual/recurrent gliomas. *Chin Med J (Engl)* 2012; 125: 91–96.

141. Van Laere K, Ceyssens S, Van Calenbergh F, *et al.* Direct comparison of 18F-FDG and ^{11}C-methionine PET in suspected recurrence of glioma: sensitivity, inter-observer variability and prognostic value. *Eur J Nucl Med Mol Imaging* 2005; 32: 39–51.

142. Chen W, Silverman DHS, Delaloye S, *et al.* 18F-FDOPA PET imaging of brain tumors: comparison study with 18F-FDG PET and evaluation of diagnostic accuracy. *J Nucl Med* 2006; 47: 904–911.

143. Oborski MJ, Demirci E, Laymon CM, *et al.* Assessment of early therapy response with 18F-FLT PET in glioblastoma multiforme. *Clin Nucl Med* 2014; 39: e431–e432.

144. Galldiks N, Langen KJ, Holy R, *et al.* Assessment of treatment response in patients with glioblastoma using O-(2-18F-fluoroethyl)-L-tyrosine PET in comparison to MRI. *J Nucl Med* 2012; 53: 1048–1057.

145. Piroth MD, Pinkawa M, Holy R, *et al.* Prognostic value of early [18F] fluoroethyltyrosine positron emission tomography after radiochemotherapy in glioblastoma multiforme. *Int J Radiat Oncol Biol Phys* 2011; 80: 176–184.

146. Li Z, Yu Y, Zhang H, *et al*. A meta-analysis comparing 18F-FLT PET with 18F-FDG PET for assessment of brain tumor recurrence. *Nucl Med Commun* 2015; 36: 695–701.

147. Kebir S, Fimmers R, Galldiks N, *et al*. Late pseudoprogression in glioblastoma: diagnostic value of dynamic O-(2-[18F]fluoroethyl)-L-tyrosine PET. *Clin Cancer Res* 2016; 22: 2190–2196.

148. Kebir S, Khurshid Z, Gaertner FC, *et al*. Unsupervised consensus cluster analysis of [18F]-fluoroethyl-L-tyrosine positron emission tomography identified textural features for the diagnosis of pseudoprogression in high-grade glioma. *Oncotarget* 2017; 8: 8294–8304.

149. Batchelor TT, Duda DG, di Tomaso E, *et al*. Phase II study of cediranib, an oral pan-vascular endothelial growth factor receptor tyrosine kinase inhibitor, in patients with recurrent glioblastoma. *J Clin Oncol* 2010; 28: 2817–2823.

150. Batchelor TT, Sorensen AG, di Tomaso E, *et al*. AZD2171, a pan-VEGF receptor tyrosine kinase inhibitor, normalizes tumor vasculature and alleviates edema in glioblastoma patients. *Cancer Cell* 2007; 11: 83–95.

151. Norden AD, Drappatz J, Muzikansky A, *et al*. An exploratory survival analysis of anti-angiogenic therapy for recurrent malignant glioma. *J Neurooncol* 2009; 92: 149–155.

152. Radbruch A, Lutz K, Wiestler B, *et al*. Relevance of T2 signal changes in the assessment of progression of glioblastoma according to the Response Assessment in Neurooncology criteria. *Neuro-Oncol* 2012; 14: 222–229.

153. Huang RY, Rahman R, Ballman KV, *et al*. The impact of T2/FLAIR evaluation per RANO criteria on response assessment of recurrent glioblastoma patients treated with bevacizumab. *Clin Cancer Res* 2016; 22: 575–581.

154. Nowosielski M, Ellingson BM, Chinot OL, *et al*. Radiologic progression of glioblastoma under therapy: an exploratory analysis of AVAglio. *Neuro-Oncol*. Epub ahead of print 2017. DOI: 10.1093/neuonc/nox162.

155. Nowosielski M, Wiestler B, Goebel G, *et al*. Progression types after antiangiogenic therapy are related to outcome in recurrent glioblastoma. *Neurology* 2014; 82: 1684–1692.

156. Cachia D, Elshafeey NA, Kamiya-Matsuoka C, *et al*. Radiographic patterns of progression with associated outcomes after bevacizumab therapy in glioblastoma patients. *J Neurooncol* 2017; 135: 75–81.

157. Gahrmann R, van den Bent M, van der Holt B, *et al*. Comparison of 2D (RANO) and volumetric methods for assessment of recurrent glioblastoma treated with bevacizumab: a report from the BELOB trial. *Neuro-Oncol* 2017; 19: 853–861.

158. Ellingson BM, Kim HJ, Woodworth DC, *et al*. Recurrent glioblastoma treated with bevacizumab: contrast-enhanced T1-weighted subtraction maps improve tumor delineation and aid prediction of survival in a multicenter clinical trial. *Radiology* 2014; 271: 200–210.

159. Ellingson BM, Cloughesy TF, Lai A, *et al*. Quantification of edema reduction using differential quantitative T2 (DQT2) relaxometry mapping in recurrent glioblastoma treated with bevacizumab. *J Neurooncol* 2012; 106: 111–119.

160. Gerstner ER, Frosch MP and Batchelor TT. Diffusion magnetic resonance imaging detects pathologically confirmed, nonenhancing tumor progression in a patient with recurrent glioblastoma receiving bevacizumab. *J Clin Oncol* 2009; 28: e91–e93.

161. Yamasaki F, Kurisu K, Aoki T, *et al*. Advantages of high b-value diffusion-weighted imaging to diagnose pseudo-responses in patients with recurrent glioma after bevacizumab treatment. *Eur J Radiol* 2012; 81: 2805–2810.

162. Rieger J, Bähr O, Müller K, *et al*. Bevacizumab-induced diffusion-restricted lesions in malignant glioma patients. *J Neurooncol* 2010; 99: 49–56.

163. Nguyen HS, Milbach N, Hurrell SL, *et al*. Progressing bevacizumab-induced diffusion restriction is associated with coagulative necrosis surrounded by viable tumor and decreased overall survival in patients with recurrent glioblastoma. *AJNR Am J Neuroradiol* 2016; 37: 2201–2208.

164. Zhang M, Gulotta B, Thomas A, *et al*. Large-volume low apparent diffusion coefficient lesions predict poor survival in bevacizumab-treated glioblastoma patients. *Neuro-Oncol* 2016; 18: 735–743.

165. Pope WB, Qiao XJ, Kim HJ, *et al*. Apparent diffusion coefficient histogram analysis stratifies progression-free and overall survival in patients with recurrent GBM treated with bevacizumab: a multi-center study. *J Neurooncol* 2012; 108: 491–498.

166. McDonald CR, Delfanti RL, Krishnan AP, *et al*. Restriction spectrum imaging predicts response to bevacizumab in patients with high-grade glioma. *Neuro-Oncol* 2016; 18: 1579–1590.

167. Kickingereder P, Wiestler B, Graf M, *et al*. Evaluation of dynamic contrast-enhanced MRI derived microvascular permeability in recurrent glioblastoma treated with bevacizumab. *J Neurooncol* 2015; 121: 373–380.

168. Stecco A, Amatuzzo P, Sponghini AP, *et al*. Prognostic value of relative cerebral blood volume (rCBV) in patients with recurrent glioblastoma multiforme treated with bevacizumab. *J Neurosurg Sci*. Epub ahead of print 2016.

169. Leu K, Boxerman JL, Lai A, *et al*. Bidirectional contrast agent leakage correction of dynamic susceptibility contrast (DSC)-MRI improves cerebral blood volume estimation and survival prediction in recurrent glioblastoma treated with bevacizumab. *J Magn Reson Imaging* 2016; 44: 1229–1237.

170. Schmainda KM, Zhang Z, Prah M, *et al*. Dynamic susceptibility contrast MRI measures of relative cerebral blood volume as a prognostic marker for overall survival in recurrent glioblastoma: results from the ACRIN 6677/RTOG 0625 multicenter trial. *Neuro-Oncol* 2015; 17: 1148–1156.

171. Hutterer M, Nowosielski M, Putzer D, *et al*. O-(2-18F-fluoroethyl)-L-tyrosine PET predicts failure of antiangiogenic treatment in patients with recurrent high-grade glioma. *J Nucl Med* 2011; 52: 856–864.

172. Galldiks N, Rapp M, Stoffels G, *et al*. Response assessment of bevacizumab in patients with recurrent malignant glioma using [18F] fluoroethyl-L-tyrosine PET in comparison to MRI. *Eur J Nucl Med Mol Imaging* 2013; 40: 22–33.

173. Galldiks N, Rapp M, Stoffels G, *et al*. Earlier diagnosis of progressive disease during bevacizumab treatment using O-(2-18F-fluorethyl)-L-tyrosine positron emission tomography in comparison with magnetic resonance imaging. *Mol Imaging* 2013; 12: 273–276.

174. Hodi FS, O'Day SJ, McDermott DF, *et al*. Improved survival with ipilimumab in patients with metastatic melanoma. *N Engl J Med* 2010; 363: 711–723.

175. Robert C, Long GV, Brady B, *et al*. Nivolumab in previously untreated melanoma without BRAF mutation. *N Engl J Med* 2015; 372: 320–330.

176. Robert C, Ribas A, Wolchok JD, *et al*. Anti-programmed-death-receptor-1 treatment with pembrolizumab in ipilimumab-refractory advanced melanoma: a randomised dose-comparison cohort of a phase 1 trial. *Lancet* 2014; 384: 1109–1117.

177. Okada H, Kohanbash G, Zhu X, *et al*. Immunotherapeutic approaches for glioma. *Crit Rev Immunol* 2009; 29: 1–42.

178. Hamid O, Robert C, Daud A, *et al*. Safety and tumor responses with lambrolizumab (anti-PD-1) in melanoma. *N Engl J Med* 2013; 369: 134–144.

179. Brahmer JR, Tykodi SS, Chow LQM, *et al*. Safety and activity of anti-PD-L1 antibody in patients with advanced cancer. *N Engl J Med* 2012; 366: 2455–2465.

180. Okada H, Weller M, Huang R, *et al*. Immunotherapy response assessment in neuro-oncology: a report of the RANO working group. *Lancet Oncol* 2015; 16: e534–e542.

181. Sampson JH, Heimberger AB, Archer GE, *et al*. Immunologic escape after prolonged progression-free survival with epidermal growth factor receptor variant III peptide vaccination in patients with newly diagnosed glioblastoma. *J Clin Oncol* 2010; 28: 4722–4729.

182. Kebir S, Rauschenbach L, Galldiks N, *et al*. Dynamic O-(2-[18F]fluoroethyl)-L-tyrosine PET imaging for the detection of checkpoint inhibitor-related pseudoprogression in melanoma brain metastases. *Neuro-Oncol* 2016; 18: 1462–1464.

183. Antonios JP, Soto H, Everson RG, *et al*. Detection of immune responses after immunotherapy in glioblastoma using PET and MRI. *Proc Natl Acad Sci USA* 2017; 114: 10220–10225.

184. Ellingson BM, Bendszus M, Boxerman J, *et al*. Consensus recommendations for a standardized brain tumor imaging protocol in clinical trials. *Neuro-Oncol* 2015; 17: 1188–1198.

185. Welker K, Boxerman J, Kalnin A, *et al*. ASFNR recommendations for clinical performance of MR dynamic susceptibility contrast perfusion imaging of the brain. *AJNR Am J Neuroradiol* 2015; 36: E41–E51.

186. Rios Velazquez E, Meier R, Dunn WD, *et al*. Fully automatic GBM segmentation in the TCGA-GBM dataset: prognosis and correlation with VASARI features. *Sci Rep* 2015; 5: 16822.

187. Korfiatis P, Kline TL and Erickson BJ. Automated segmentation of hyperintense regions in FLAIR MRI using deep learning. *Tomogr J Imaging Res* 2016; 2: 334–340.

188. Meier R, Porz N, Knecht U, *et al*. Automatic estimation of extent of resection and residual tumor volume of patients with glioblastoma. *J Neurosurg* 2017; 127: 798–806.

189. Meier R, Knecht U, Loosli T, *et al*. Clinical evaluation of a fully-automatic segmentation method for longitudinal brain tumor volumetry. *Sci Rep* 2016; 6: 23376.

190. Kamnitsas K, Ledig C, Newcombe VFJ, *et al*. Efficient multi-scale 3D CNN with fully connected CRF for accurate brain lesion segmentation. *Med Image Anal* 2017; 36: 61–78.